Earth Planet. Sci. Lett. 663 (2025) 119409

Contents lists available at ScienceDirect

Earth and Planetary Science Letters

journal homepage: www.elsevier.com/locate/epsl

Duration of isobaric heating and slab rollback in the Aegean extensional province, Eastern Mediterranean: Evidence from garnet diffusion modelling

Alexandre Peillod [a,*], Benjamin Hess [b], Evangelos Moulas [c], Simon Hector [d], Clifford G.C. Patten [e], Aratz Beranoaguirre [d], Uwe Ring [a]

[a] Department of Geological Sciences, Stockholm University, Sweden
[b] Department of Earth Sciences, University of Oxford, Oxford, UK
[c] Mainz Institute of Multiscale Modelling (M3ODEL) and Institute of Geosciences, Johannes-Gutenberg University of Mainz, Germany
[d] Chair of Geochemistry & Economic Geology, Karlsruhe Institute of Technology (KIT), Germany
[e] Institute of Mineralogy and Petrography, University of Innsbruck, Austria

ARTICLE INFO

Keywords:
Garnet diffusion chronometry
Cycladic blueschist unit
Aegean extensional province
Isobaric heating
Exhumation
Orogeny
Heat source

ABSTRACT

A phase of isobaric heating during exhumation of high-pressure rocks is often reported, but the tectonic significance of isobaric heating remains uncertain. Constraining the timescales of isobaric heating is essential for connecting the heating to tectonic processes of lithospheric thickening and extension. An isobaric heating phase has been reported for the Cycladic Blueschist Unit in the Hellenide orogen of Greece. We present diffusion modeling of major elements in garnet using data from Naxos Island to provide new independent estimates of the duration of isobaric heating. We also present radioactive trace element analyses of the Cycladic basement and a heat conduction model to explore the heat production generated in the basement and its influence on isobaric heating. Our model indicates that isobaric heating occurred over ~9.7 Myr, during which the Cycladic basement generated enough heat to explain the observed temperature increase. At the end of this heating phase, the temperature increase caused a significant drop in crustal strength, which controlled the style of crustal extensional deformation during subsequent rollback of the subducting slab. Our work implies that the underthrusting of radiogenic material in convergent settings produces sufficient heat to significantly increase temperature which weakens the crust and enables pervasive deformation.

1. Introduction

Pressure-temperature (*P-T*) paths commonly reflect burial followed by exhumation due to vertical movement in the lithosphere (e.g. England and Thompson, 1984). However, a temperature increases at mid/lower-crustal depths during overall exhumation is often reported from various high-*P* (HP) units leading to β-shaped *P-T* paths, i.e., *P-T* paths characterized by heating during decompression/exhumation (Fig. 1). Examples include the Bohemian Massif (e.g. Perraki and Faryad, 2014), Alps (e.g. Bovay et al., 2022), Cyclades and Turkey (e.g. Laurent et al., 2018; Parra et al., 2002; Peillod et al., 2021a), eastern Dabie Shan (e.g. Liu et al., 2013), Himalaya (e.g. Wilke et al., 2010) and south-eastern Papua New Guinea (e.g. Faryad et al., 2019). Such isobaric heating demands that the rocks either halted or moved horizontally during their journey toward the Earth's surface (e.g. Schenker et al., 2012). The heat source for isobaric heating is not well known and various mechanisms have been suggested, such as radiogenic heat production following the accretion of continental material (e.g. Borghi et al., 1996; Wiederkehr et al., 2008); slab breakoff (e.g. Shizova et al., 2019); mantle delamination (e.g. Henk et al., 2000), or horizontal flow of the lower crust during slab rollback (Huet et al., 2011). Based on two-dimensional numerical modelling, Sizova et al. (2019) proposed that upwelling of hot asthenospheric mantle following slab rollback or slab breakoff causes β-shaped *P-T* paths. The authors further suggested that the heat associated with the upwelling mantle explains a variety of *P-T* paths from many collisional orogens (see examples above).

In the Aegean extensional province, it was speculated that isobaric heating was associated with horizontal ductile flow (Huet et al., 2011; Scheffer et al., 2016). However, pronounced flow of mid/lower-crustal rocks is strongly aided by high temperatures and the presence of melt (Arzi, 1978; Rosenberg and Handy, 2005; Vanderhaeghe, 2012). Hence, it appears more likely that ductile flow was not significant at the

* Corresponding author at:
E-mail address: alexandre.peillod@gmail.com (A. Peillod).

https://doi.org/10.1016/j.epsl.2025.119409
Received 23 October 2024; Received in revised form 22 February 2025; Accepted 1 May 2025
Available online 15 May 2025

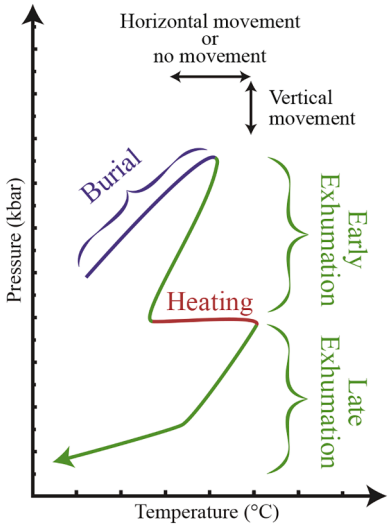

Fig. 1. Schematic *P-T* path showing burial and peak HP metamorphism followed by two exhumation stages separated by an isobaric heating stage.

beginning but at the end of isobaric heating. Therefore, the tectonic significance of isobaric heating during exhumation is not well understood, and critical tectonic questions remain, such as to what the timescales and tectonic consequences of isobaric heating are.

We address the tectonic significance of isobaric heating in the middle/lower crust of the Aegean extensional province in the Eastern Mediterranean (Fig. 2a), where isobaric heating is of regional importance (Huet et al., 2015; Laurent et al., 2018; Parra et al., 2002; Peillod et al., 2021a; Ring et al., 1999; Scheffer et al., 2016; van der Maar and Jansen, 1983) (Fig. 2a and Table 1). On the island of Naxos in the central Aegean, this phase is resolved at various levels of the structural section (Fig. 2b and Table 1) after 32 Ma. The available age data from the central Aegean show that the start of isobaric heating predated the onset of slab-rollback-controlled large-scale lithospheric extension by almost 10 Ma (Peillod et al., 2024, 2021a; Villa et al., 2023). We conducted diffusion modelling on chemically zoned garnet from Naxos to provide new independent estimates for the duration of both isobaric heating and subsequent exhumation. Constraining the timescales of these events is an essential first step for connecting previously determined *P-T* paths (Fig. 3b-e) to tectonic processes of lithospheric thickening and ensuing slab-rollback-controlled extension.

2. Setting

The Aegean region in the Hellenides is a well-studied natural laboratory for understanding subduction-related burial, HP metamorphism and exhumation of the Cycladic Blueschist Unit (CBU). The CBU comprises continental fragments of the Adriatic Plate and can be divided into three nappes: the Upper-, Middle-, and Bottom-CBU nappes, which

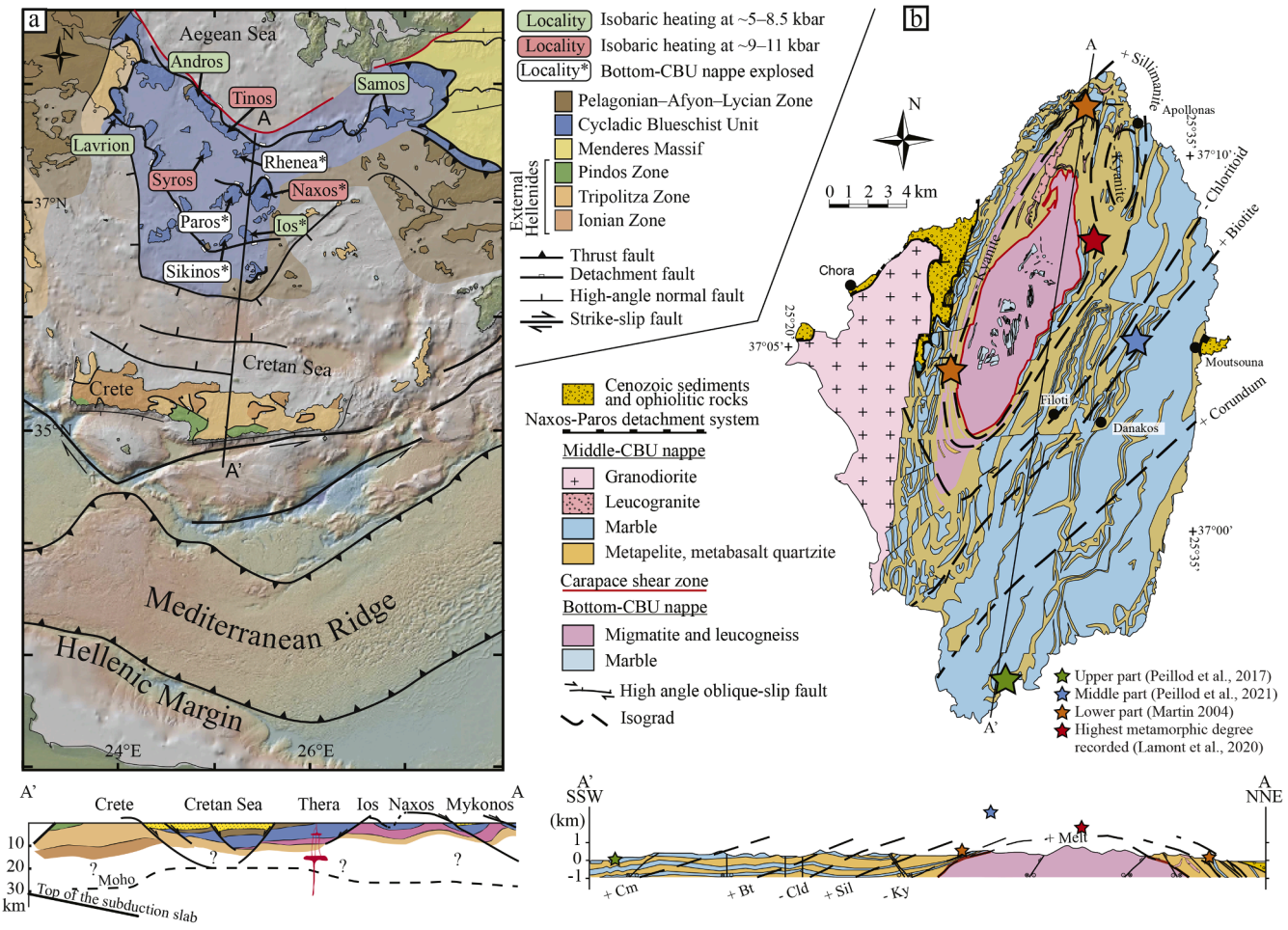

Fig. 2. a) Simplified tectonic map and cross section of the Aegean showing the major tectonic units (modified from Jolivet et al., 2010). b) Geological map of Naxos with isograd pattern (Jansen and Schuiling, 1976; Vanderhaeghe et al., 2007). Blue star is the sample locality for which the diffusion model is performed and green, brown and red stars are sample locations of previous petrologic studies. Cross-section showing the domal architecture of Naxos with sample localities projected into the cross-section plane.

Table 1
P-T estimates and thermal changes for isobaric heating in Cyclades.

Locality	Heating interval (°C)	Δ (°C)	Pressure (kbar)	Thermal gradient interval (°C/km)	Δ Thermal gradient (°C/km)	References
Andros	300–420	120	7.0	12–16	5	Huet et al. (2015)
Lavrion	300–350	50	5.0–8.5	12–14	2	Scheffer et al. (2016)
Ios	380–420	40	6.0–7.0	10–12	2	van der Maar and Jansen (1983)
Samos	390–470	80	7.0	15–18	3	Ring et al. (1999)
Tinos	400–550	150	9.0	12–17	5	Parra et al. (2002)
Syros	500–570	70	10.0	14–16	2	Laurent et al. (2018)
Naxos	519–584	65	9.0	16–18	2	Peillod et al. (2021a)
	550–625	75	10.0	15–17	2	Martin (2004)
	590–700	110	9.0–10.9	16–19	3	Lamont et al. (2020)

experienced HP metamorphism at 55–45, 45–38, and 34–28 Ma, respectively (Glodny and Ring, 2022, and references therein). While a structurally deeper nappe is underthrusting, the nappe above it is being exhumed into the middle crust, e.g., the Middle-CBU nappe was exhumed and emplaced over the underthrusting Bottom-CBU nappe at 32–28 Ma (Forster et al., 2020; Peillod et al., 2017).

At lower structural levels of the Middle-CBU Nappe, an isobaric heating stage has been reported which occurred at higher *P-T* conditions in the center than at the periphery of the Cycladic archipelago (Fig. 2a and Table 1). After the initial subduction/exhumation cycle in the subduction channel during lithospheric shortening, the CBU underwent rollback-controlled lithospheric extension, associated with a greenschist/amphibolite-facies metamorphic overprint (with local anatexis) starting during the early Miocene at 23–19 Ma (e.g. Bakowsky et al., 2023; Grasemann et al., 2012; Ring et al., 2010). The phase of extension-controlled exhumation was more pronounced where isobaric heating occurred at deeper crustal levels in the central Cyclades (Fig. 2a).

The island of Naxos (Fig. 2b) exposes the Middle- and Bottom-CBU nappes. The Middle-CBU nappe, comprising metapelite, amphibolite and marble, reached peak HP metamorphism during the Eocene at 42–38 Ma (e.g. Villa et al., 2023; Wijbrans and McDougall, 1988) and was subsequently exhumed and thrust over the subducting Bottom-CBU nappe during the Oligocene at ~32–28 Ma (Peillod et al., 2017). The latter represents Carboniferous granitic basement with minor metapelite and marble (e.g. Lister and Forster, 1996). The metamorphic grade increases from the top to the bottom of the structural section (Fig. 2b and 3a).

At the top of the section, the rocks do not show isobaric heating (Fig. 3b; Peillod et al., 2017), however, a discrete pre-Miocene thermal pulse at low P (~4 kbar) was suggested from $^{40}Ar/^{39}Ar$ step-heating analyses (Cao et al., 2018), and by the rare observation of biotite replacing chlorite (Lamont et al., 2020; Martin, 2004). This alleged thermal pulse was never quantified, suggesting that the temperature increase is below the accuracy of geothermobarometry methods (e.g. <20–30 °C). Lower in the section, at about the biotite isograd (Fig. 2b and Fig. 3a), isobaric heating recorded by *P-T* data is first detected (Fig. 3c; Peillod et al., 2021a). Even lower in the section, Martin (2004) also reported a stage of isobaric heating (Fig. 3d). Lamont et al. (2020) sampled at the bottom of the Middle CBU-Nappe, where the early HP loop is not observed anymore, and suggested a prograde Barrovian-type *P-T* path based on garnet isopleths from thermodynamic modeling performed on one sample (TL67). Other thermobarometric methods applied to sample TL67 did not support initially increasing *P* and *T*, and the *P-T* path from another sample (TNL22) shows near isobaric heating. Lamont et al. (2020) interpreted the lack of a HP overprint in the lower part of the Middle-CBU nappe to indicate that this lower part represents a separate, non-HP tectonic unit. They further speculated that the HP upper part of the Middle-CBU nappe thrust onto the non-HP unit along the large-displacement Eocene/Oligocene Zas shear zone. Structural work in the Zas shear zone reveals Miocene greenschist top-to-the-NNE extensional shearing with no significant strain localization into the shear zone (Peillod et al., 2021b). Moreover, Naxos is known to expose an anomalous large number of metabauxite deposits, which occur within the entire Middle-CBU nappe across the alleged Zas shear zone (Bonneau et al., 1978; Feenstra, 1985; Hecht, 1979), strongly suggesting that the

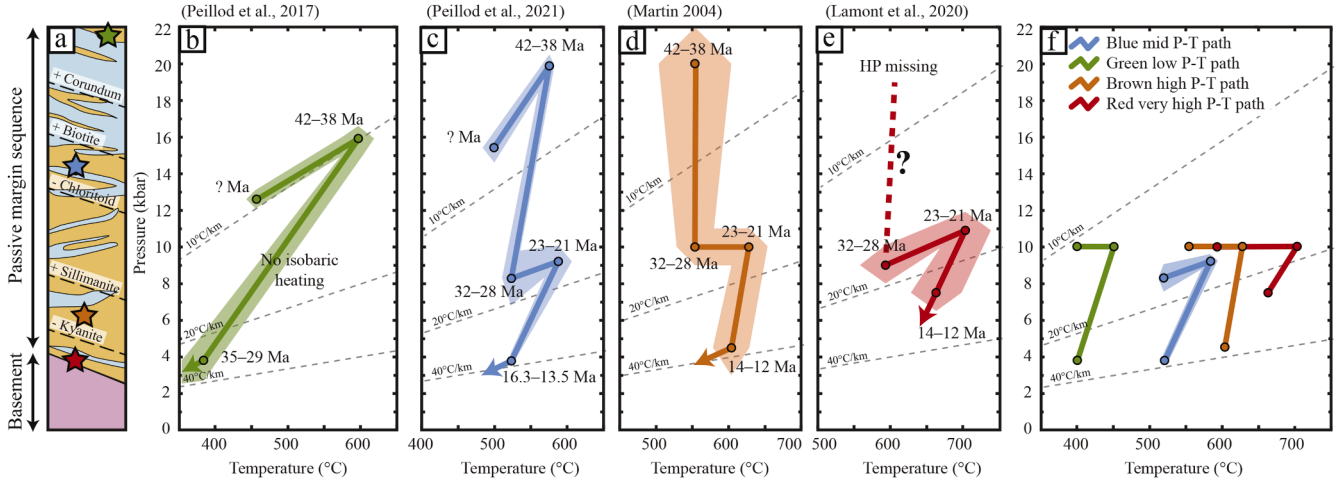

Fig. 3. a) Schematic tectonostratigraphic column showing relative position of analyzed samples. b-e) Published *P-T* paths (Lamont et al., 2020; Martin, 2004; Peillod et al., 2021a, 2017). Ages displayed on the *P-T* paths are from Peillod et al. (2024, 2021a). Note that the intensity of isobaric heating increases toward the bottom of the Middle-CBU nappe and that the HP *P-T* path segment is missing at the highest metamorphic grade in (e). f) Four modelled paths that mimic the isobaric paths in Naxos. Note that for the coolest path (green) there is no isobaric heating observed, however, we modeled a hypothetic isobaric path (Model 2; Low *P-T* path) to understand the timing needed for chemical garnet diffusion times scales at such low temperatures.

Middle-CBU nappe represents one single, coherent tectonic unit. Chemical and $\delta^{18}O$ isotope data of garnet cores and rims, as well as the LREE-rich composition of epidote are interpreted to reflect HP metamorphism of the lower part of the Middle-CBU nappe (Duchêne et al., 2006; Martin et al., 2006). Thermodynamic models show peak HP metamorphism followed by early exhumation, isobaric heating and subsequent exhumation (Martin, 2004). Following these arguments, Peillod et al. (2021b) reinterpreted the Lamont et al. (2020) data as reflecting isobaric heating following a completely erased earlier HP *P-T* segment (Fig. 3e). After isobaric heating, exhumation of the lower crust during slab rollback occurred in two steps, near isothermally at 23–12 Ma followed by pronounced cooling until ~6 Ma (e.g. Brichau et al., 2006; Peillod, 2018; Ring et al., 2018; Wijbrans and McDougall, 1988).

3. Methodology

3.1. Diffusion modeling

The garnet that shows the "coldest" isobaric heating path on Naxos (blue *P-T* path in Fig. 3c) exhibits distinct, chemical zones that can provide constraints on the duration of isobaric heating via diffusion modeling (Fig. 4; see Peillod et al. (2021a) for more details). The garnet comprises a core, inner, central, and outer rim, mainly defined from almandine and spessartine chemical profiles (Fig. 4a-e), with the last two chemical zones having formed during isobaric heating and subsequent exhumation, respectively.

We conduct numerical simulations of garnet diffusion that integrate the *P-T* uncertainties using a Monte Carlo approach (Model 1, Mid *P-T* path; Fig. 3f). Our approach is used to determine the best-fit timescale for isobaric heating and subsequent exhumation based on chi-square minimization (reported as mean and 1σ standard deviations; Figs. 5a and Fig. S1 in supplementary data item). We approximate the garnet as spherical and solve the radial diffusion equation for almandine–pyrope–grossular–spessartine diffusion using the forward time-centered space (FTCS) method (see supplementary data item for further details).

The garnet profile being modeled is divided into the four segments described above. The initial condition assumes that the central rim grows instantly at the beginning of the isobaric heating phase (519 ± 6 °C and 8.3 ± 0.75 kbar, 1σ uncertainties) with an initially sharp chemical contact (Fig. 4f). The core and inner rim are assumed to have formed during previous metamorphic stages. Diffusion occurs as T and P linearly increase to peak T after isobaric heating. The outer rim grows at peak conditions (584 ± 9.5 °C and 9.2 ± 0.9 kbar) and then T and P linearly decrease during the exhumation phase (Fig. 5). The final conditions are 520 ± 2 °C and 3.8 ± 0.15 kbar. A video showing the evolving chemical profile during heating and exhumation is provided in Figure S2.

The uncertainties on the given temperature and pressure of each stage are used in a Monte Carlo simulation to estimate the uncertainty on the stage durations. The mean and standard deviations of the pressure and temperature values are used to generate 100,000 sets of different *P-T* conditions. Then for each set of *P-T* conditions, we trial 1000 different combinations of timescales for isobaric heating and late exhumation. The best-fit timescale is determined based on chi-square minimization between the observed and modeled almandine and spessartine profiles. The results provide the duration of each stage with uncertainties (Figs. 5a and S1). More details of the method are provided in the supplementary data item.

For comparison, we also determine the best-fit timescales using

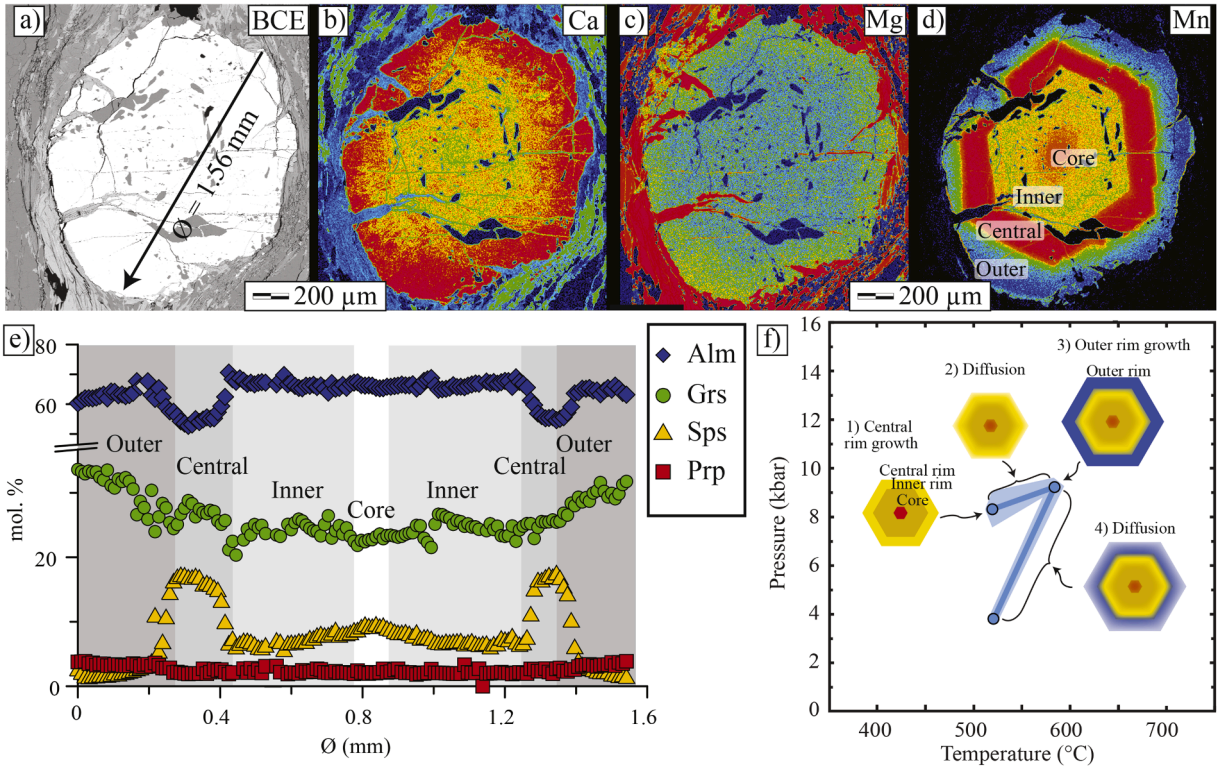

Fig. 4. a) SEM images of garnet from sample NP39 (37°05′1″N,25°33′07″E). b-d) Zoning maps and; e) element profiles of representative garnet porphyroblasts (sample NP39) after Peillod et al. (2021a). XFe (Alm) = Fe/(Mg + Ca + Fe + Mn); XCa (Grs) = Ca/(Mg + Ca + Fe + Mn); XMn (Sps) = Mn/(Mg + Ca + Fe + Mn); XMg (Prp) = Mg/(Mg + Ca + Fe + Mn). Garnet core and rims are defined by Mn composition maps and profiles. (f) Overview of garnet growth and element diffusion during isobaric heating and exhumation phases. Garnet core and inner rims grow during prograde and peak HP metamorphism whereas garnet central rim grows at the end of the early exhumation. Diffusion occurs during *P* and *T* increase as garnet core, inner and central rim grew. The outer rim grows at peak metamorphism and then diffusion occurs for all garnet rims during *P* and *T* decrease.

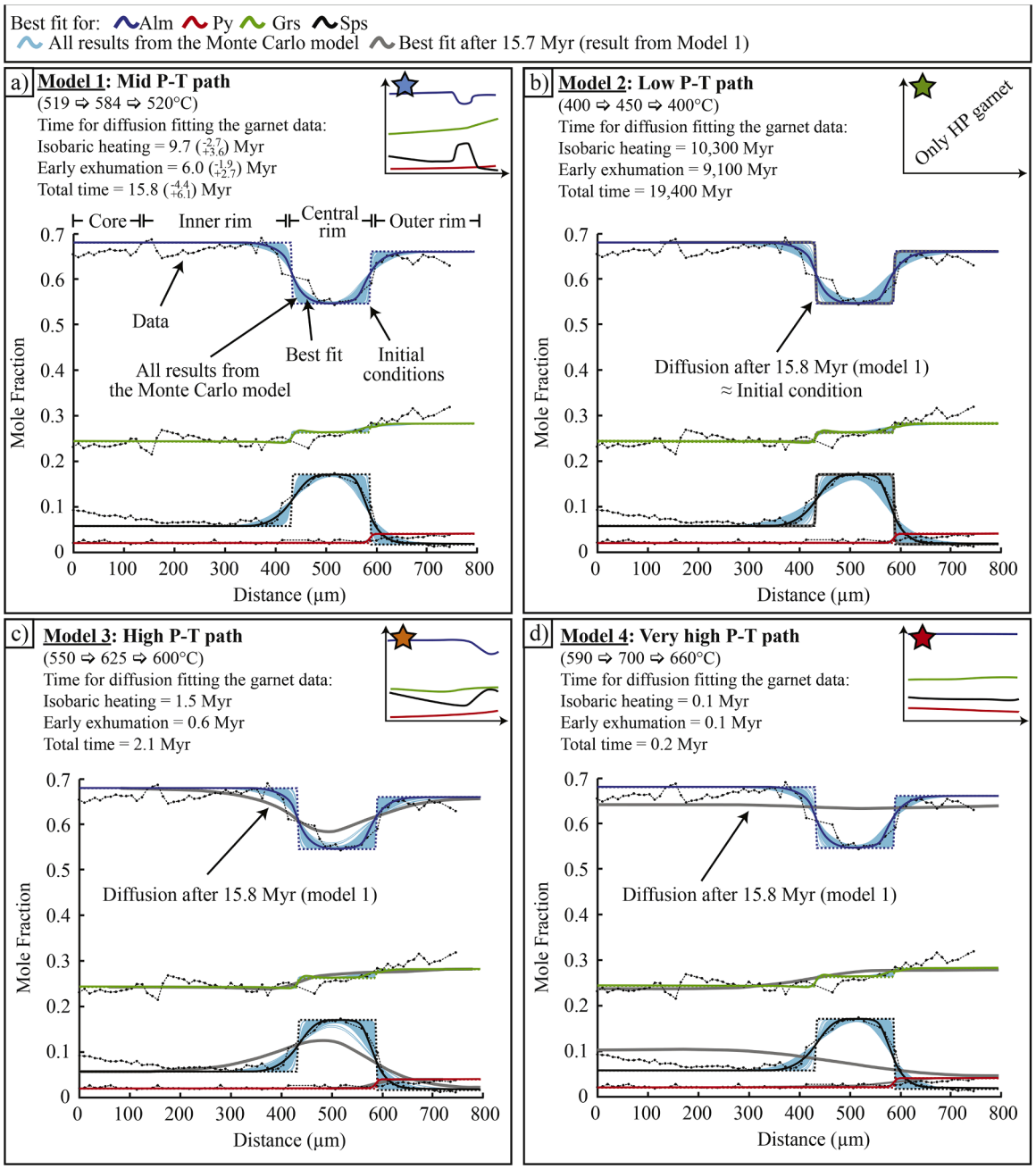

Fig. 5. Diffusion models for the four *P-T* paths shown in Fig. 3 using the garnet from sample NP39 (Peillod et al. (2021a). a) Diffusion model results using the *P-T* path determined by Peillod et al. (2021a). b-d) Model results using *P-T* paths with lower *T* (Model 2) and higher *T* (Model 3 and 4) set in Fig. 3. Inserts correspond to typical garnet chemical profiles observed on Naxos for each *P-T* path in Fig. 3. Note the similarities between the garnet chemical profiles after 15.8 Myr in models 3 and 4 with garnet chemical profiles observed on Naxos.

diffusion modeling for the three other *P-T* paths shown in Fig. 3f (green low-*T* path, brown high-*T* and red very-high-*T* paths; models 2, 3 and 4 respectively) corresponding to the uppermost and lower parts of the Middle-CBU nappe. We test 100,000 combinations of timescales to determine the best-fit for each assumed *P-T* path. In addition, we plot the simulated extent of diffusion for the timescale determined from Model 1 (grey lines in Figs. 6b-d) to compare it with other garnet chemical profiles observed in Naxos (insets in Fig. 5).

3.2. Assumptions in diffusion methodology

Our diffusion model assumes instantaneous garnet growth and initially sharp chemical contacts. Deviations from these assumptions could impact our results, and therefore, we explore these assumptions.

If rim growth was delayed or sluggish relative to diffusion at the start of the model, then the timescales we determine would be underestimated. Garnet central rim likely started to grow at the beginning of isobaric heating. As the composition of the central rim was used to determine the initial pressure and temperature conditions at the start of isobaric heating (Peillod et al., 2021a), it is reasonable to assume that the entire rim grew at or near these conditions (i.e., at the start of the model). This is also consistent with the presence of chlorite and ilmenite throughout the central rim which were only stable early in the isobaric heating stage (Peillod et al., 2021a). As diffusion rate increases with temperature, diffusion would have been sluggish at the beginning of the isobaric heating stage when the garnet rim was growing. Consequently,

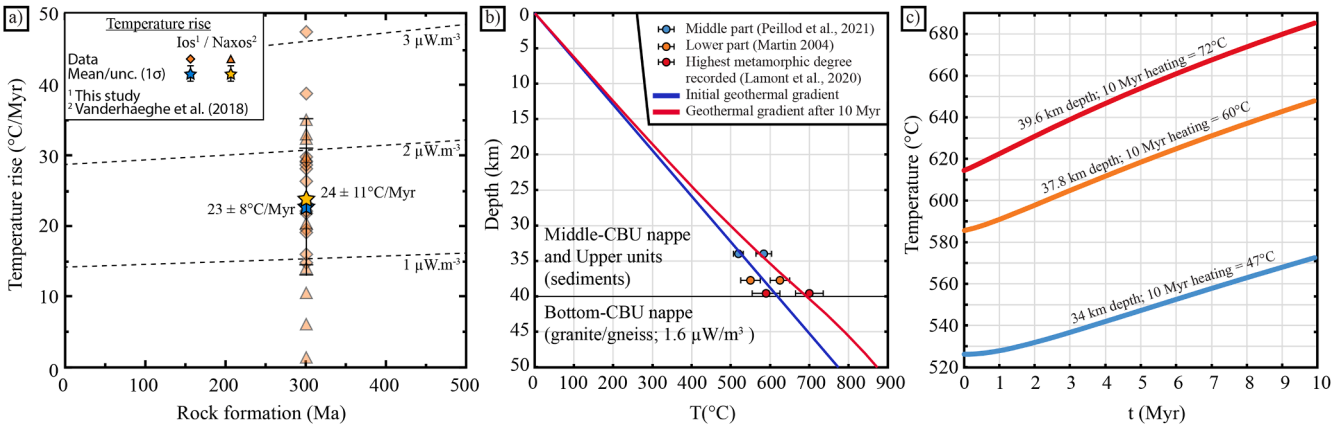

Fig. 6. a) Temperature rise per Myr versus rock formation in function of the heat production in a closed system (Ryan and Dewey, 2019) for granite, gneiss, schist and metabasalt in the Lower-CBU nappe from Ios (this study) and from Naxos (from Vanderhaeghe et al., 2018). Age formation of the rocks within the Lower-CBU nappe is set at 300 Ma following detrital ages (Reischmann, 1998; Keay et al., 2001; Vanderhaeghe et al., 2018; Zlatkin et al., 2018; Flansburg et al., 2019). b) 1-D conductive model for 10 Myr heating resulting from radiogenic decay of 10 km thick granitic/gneiss body. Result of the simulation with comparison of the temperature ranges of the isobaric heating observed in Naxos. c) Temperature increase over time from three points located at 34, 37.8 and 39.6 km depth.

the rim can be treated as having effectively grown instantaneously for the purposes of our model.

We also assume initially sharp contacts as is standard in diffusion modeling. Any initial curvature in the zone contacts would lead to a shorter true timescale for the observed extent of diffusional relaxation compared to the assumption of an initially sharp contact. The formation of the outer rim may have involved partial resorption of the central rim and regrowth near the maximum temperature which could lead to asymmetric and curved initial chemical profiles between garnet zones. Therefore, our timescale estimates represent maximum values. Nonetheless, given the symmetry across the central and outer rim contact (particularly of the spessartine component), we expect any initial zonation, if present, to have been short-lived relative to the overall length scale of diffusion. Otherwise, we would expect a greater degree of asymmetry to be observed. This suggests that any initial zonation would not significantly change our model results. Thus, while we note these potential complications, we consider our model assumptions and results reasonable, particularly given their consistency with independent geochronology and radiogenic heating rates (see below).

3.3. Major and radioactive trace elements geochemistry

The major element composition was measured by X-ray fluorescence (XRF) (S4 Explorer, Bruker AXS) on glass beads with BHVO-1, MRG-1, RGM-1 and SY-2 as reference material to control analytical precision and accuracy. Radioactive trace element content (^{40}K, ^{238}U, ^{232}Th) was measured by laser-ablation inductively-coupled-plasma mass-spectrometry on pressed powder pellets (PPP-LA-ICP-MS) using a Teledyne 193 nm Excimer laser coupled to an ICP-MS (Element XR ThermoFisher) with a spot size of 85 µm, laser frequency of 10 Hz, fluence of 5 J·cm^{-2}, He, Ar and N flow of 0.3 L·min^{-1}, 0.85 L·min^{-1} and 10 mL min^{-1}, respectively. Pressed powder pellets (PPP) are prepared following the method described in Patten et al. (2023). The SiO_2 content from XRF analyses was used for internal standard calibration. Calibration and data quality monitoring was done using PPP of standards BHVO-1, BHVO-2, BCR-2 and BIR-1 from the United States Geological Survey (USGS).

3.4. Heat production

Heat production values were calculated from the measured amounts of ^{238}U, ^{40}K and ^{232}Th (C_U, C_K and C_{Th}) in augengneiss, granite, micaschist and metabasite from the Bottom-CBU on Ios Island and based on the relationship originally proposed Rybach (1988):

$$A(\mu W/m^3) = \rho(0.0952\ C_U + 0.0348\ C_K + 0.0256\ C_{Th}),$$

where ρ is the density in g·cm^{-3}, and C_U, C_K and C_{Th} are mass fractions of radioactive isotopes in µg·g^{-1} (or ppm), % and µg·g^{-1}, respectively. We used an average rock density of 2700 kg·m^{-3}. The amounts of ^{238}U and ^{232}Th represent 99 % and 99.98 % of the radiogenic isotopes, which, for simplification, represent the total of all radiogenic elements. The ^{40}K amount is commonly reported as K_2O, therefore we applied a coefficient of 0.83 to convert K_2O values to K (see Artemieva et al., 2017).

3.5. 1-D heat conduction model

For the one dimensional calculation of the temperature evolution we used the openly available code T1dH (Moulas and Schorn, 2024). The T1dH code utilizes the enthalpy method and has been benchmarked versus several analytical solutions. Our model configuration assumes that the Middle-CBU nappe is instantly thrust onto the Bottom-CBU nappe during the Oligocene. The minimum pressure for the Bottom-CBU nappe and the maximum pressure for the Middle-CBU nappe in the Oligocene are estimated at ~10–11 kbar (Buick and Holland, 1989; Lamont et al., 2020), giving a depth of 40 km for the base of the Middle-CBU nappe assuming an average rock density of 2700 kg·m^{-3} and a lithostatic pressure gradient. The depth for the lower part of the Bottom-CBU nappe in the Oligocene is more difficult to estimate. However, erosion was very low during the Oligocene/early Miocene due to low elevation (Kuhlemann et al., 2004) suggesting that the thickness of the crust did not exceed 50 km. Therefore, the thickness of the Bottom-CBU nappe was set at 10 km and erosion was not included in our modelling.

The major heat sources are assumed to be the decay of radioactive elements in the continental basement of the Bottom-CBU nappe, and also the heat transferred to the base of the crust from the upper mantle. Heat transfer is assumed to be conductive having constant thermal conductivity (equal to 2.0 W/m/K). The specific heat capacity is considered to be 1050 (J/K/kg) and the volumetric rate of radiogenic heat production was set to 1.6 µW·m^{-3}. The basal heat flux was set to be 30.5mW·m^{-2}.

4. Duration of isobaric heating and subsequent exhumation

The central rim of the garnet in model 1 (blue *P-T* path; Fig. 5a) grows at 519 ± 6 °C and 8.3 ± 0.75 kbar (1σ uncertainties) and then heats up linearly to 584 ± 9.5 °C (Tmax) at 9.2 ± 0.9 kbar. Our model results indicate a 9.7 −2.7/+3.6 Myr duration for this heating stage.

After the end of isobaric heating, the garnet outer rim grows at *P-T* conditions of 584 ± 9.5 °C and 9.2 ± 0.9 kbar. During subsequent exhumation, cooling to 520 ± 2 °C and 3.8 ± 0.15 kbar occurs at a linear rate. The model gives a duration of 6.0 −1.9/+2.7 Myr for this stage. The combined duration of these two stages is 15.8 −4.4/+6.1 Myr.

For comparison, we also determine timescales for each stage that would be consistent with observed diffusion in the garnet chemical profile using other *P-T* paths determined for different sections of the CBU. For model 2 (green low-*T* path; Fig. 5b), diffusion would need to occur over an unrealistic period of time (>10,000 Myr, Fig. 5b) to reproduce the observed chemical relaxation. Essentially no chemical relaxation occurs at temperatures <450 °C for the total time period of 15.8 Myr derived in model 1 for the entire time for isobaric heating and subsequent exhumation. In models 3 and 4, the modeled duration of isobaric heating and exhumation is much shorter (0.16–2.1 Myr; Fig. 5c, d). Over the period of 15.8 Myr calculated for model 1, the model predicts chemical profiles that are far more relaxed than what is observed (grey profiles; Fig. 5c and d). For the very-high-temperature *P-T* path, the modelled chemical profile is almost flat (Fig. 5d).

5. Radioactive heat production of bottom-cbu nappe and 1-D conductive model

As the Middle-CBU nappe was exhumed and emplaced over the underthrusting Bottom-CBU nappe during the Oligocene (Forster et al., 2020; Peillod et al., 2017), radiogenic decay in the basement of the Bottom-CBU nappe is a potential candidate for the cause of heating. This basement is exposed only in few places in the Cyclades (Ios, Naxos, Paros, Sikinos and Rhenea islands; inset in Fig. 2a). Rocks within the Bottom-CBU nappe comprise Cambrian-Silurian garnet-mica schist and dolomitic marble intruded by Carboniferous granites (Flansburg et al., 2019; Keay et al., 2001; Reischmann, 1998; Vanderhaeghe et al., 2018; Zlatkin et al., 2018). Therefore, rocks of the Bottom-CBU nappe from Naxos and Ios are similar, except that the rocks from Naxos underwent partial melting during the Miocene. To avoid potential post-crystallization Pb loss and U gain due to the pronounced thermal overprint and deformation-enhanced fluid migration on Naxos (Henjes-Kunst et al., 1988), we determined major and trace elements from the non-melted Bottom-CBU nappe on Ios island as a proxy for the Naxos Bottom-CBU nappe (see supplementary data item). We compare the Ios data with published data from the Bottom-CBU nappe on Naxos (Vanderhaeghe et al., 2018). From the radiogenic decay in the granitic basement of the Bottom-CBU nappe, we determine heat production and performed a 1-D conductive model (Fig. 6 and Table S2).

The Th, U, and K abundances, calculated heat production values, Th/U and K/U ratios, and the temperature rise for individual samples are given in Fig. 6a and Table S2 in the supplementary data item. The heat production of all samples gives a mean value of 1.5 ± 0.5 μW/m^3 (1σ; Fig. 6a; Table S2), which corresponds to a temperature-increase rate of 23 ± 8 °C/Myr for the Bottom-CBU nappe of Ios island (Fig. 6a; Table S2) which is similar to what is reported for the Bottom-CBU nappe in Naxos (Vanderhaeghe et al., 2018).

A simple 1-D conductive model shows that 10 Myr of thermal relaxation of the Bottom-CBU nappe would be enough to isobarically increase *T* by 50–70 °C at the base of the Middle-CBU nappe (34–40 km depth, Fig. 6b and c). These model results agree with the *T* increase and its duration calculated for isobaric heating in Naxos (Fig. 5a). In contrast, the *T* increase is negligible at the top of the Middle-CBU nappe (~7–14 °C at depths of 14–20 km, Fig. 6b).

6. Discussion

6.1. Diffusion model results and naxos P-T data

The estimated duration for isobaric heating (9.7 −2.7/+3.6 Myr) and subsequent cooling during exhumation (6.0 −1.9/+2.7 Myr; total 15.8 −4.4/+6.1 Myr) is consistent with geochronologic data (Peillod et al., 2021a; Table 2). Applying the duration of isobaric heating and cooling estimated by model 1 (~15.8 Myr) to models 3 and 4 would predict chemical profiles that are far more relaxed than observed. Such highly relaxed chemical profiles have been observed in garnet from the lowermost Middle-CBU nappe, where peak-*T* exceeds 600–650 °C (Lamont et al., 2020; Martin, 2004; Peillod, 2018). High-*T* conditions (≥600–650 °C) enduring for ≥10 Myr can partially or fully eliminate chemical zonation in garnet (Caddick et al., 2010). Mn diffuses most rapidly, followed by Mg, Fe, and Ca (Borinski et al., 2012). The homogenization of older chemical zones in garnet can add uncertainties in thermodynamic models for early metamorphic stages and discrepancies in *P-T* results between different geothermobarometric methods (Peillod et al., 2021a). Lamont et al. (2020) described a garnet core from the lower part of the Middle-CBU nappe that records a Barrovian-type *P-T* path showing increasing *P* and *T* as calculated using garnet isopleths from thermodynamic model (THERMOCALC). However, results from the average *P-T* routine of THERMOCALC and combined GASP/garnet-biotite geothermobarometry do not support such a *P-T* path and are consistent with isobaric heating. It seems possible that the increasing *P-T* Barrovian-type path is the result of uncertainties due to the partial homogenization of the chemical zones in their garnet.

6.2. Heat source controlled by continental basement

The Middle-CBU nappe was thrust over the Bottom-CBU nappe at 32–28 Ma (Peillod et al., 2017; Forster et al., 2020), the latter being mainly composed of granitic gneiss. Over a period of 9.7 −2.7/+3.6 Myr determined by the diffusion modeling, we calculate that the radiogenic decay in the Bottom-CBU nappe results in a heating rate of 23 ± 8 °C/Myr, corresponding to a temperature increase of 184 ± 64 °C over ~10 Myr. Over the same period of time, isobaric heating is ~120 °C at the base (Lamont et al., 2020), ~75 °C slightly structurally above (Martin, 2004) and ~65 °C in the middle of the Naxos Middle-CBU nappe (Peillod et al., 2021a). A simple 1-D conductive heat-transfer model suggests that the radiogenic decay in the Bottom-CBU nappe alone may well explain the observed isobaric heating (Fig. 7). However, crustal-scale convection is suggested to have started at <24 Ma for the Bottom-CBU nappe (Vanderhaeghe et al., 2018) suggesting 1–4 Myr of convective heating preceding lithospheric extension (Fig. 7).

6.3. Tectonic implications of isobaric heating on large-scale extension

Our finding that thermal relaxation caused isobaric heating of the Middle-CBU nappe differs from Huet et al. (2011) and Scheffer et al. (2016) who suggested that isobaric heating was associated with horizontal ductile flow during slab rollback. These authors imply that rollback in the central Aegean Sea region commenced at the start of isobaric heating at 32–28 Ma (see also Jolivet and Brun, 2010). As argued in Huet et al. (2011), rollback-controlled extension would initially cause necking of the upper crust, which would create extensional sedimentary basins earlier than those dated at 23–19 Ma in the central Aegean (Angelier et al., 1978; Büttner and Kowalczyk, 1978; Kuhlemann et al., 2004; Roesler, 1978). Likewise, radiometric dating of extension-related

Table 2
Diffusion model results for 100,000 trials of different P-T variations and comparison with duration of isobaric heating based on geochronology data of Peillod et al. (2021a).

	Mean (Myr)	1σ uncertainty range (Myr)	Published duration from Peillod et al. (2021a) (Myr)
T1 (Isobaric heating)	**9.7**	7.1 – 13.4	4.0 – 11.0
T2 (Late exhumation)	**6.0**	4.2 – 8.7	4.7 – 10.5
Total	**15.8**	11.4 – 21.9	11.7 – 18.5

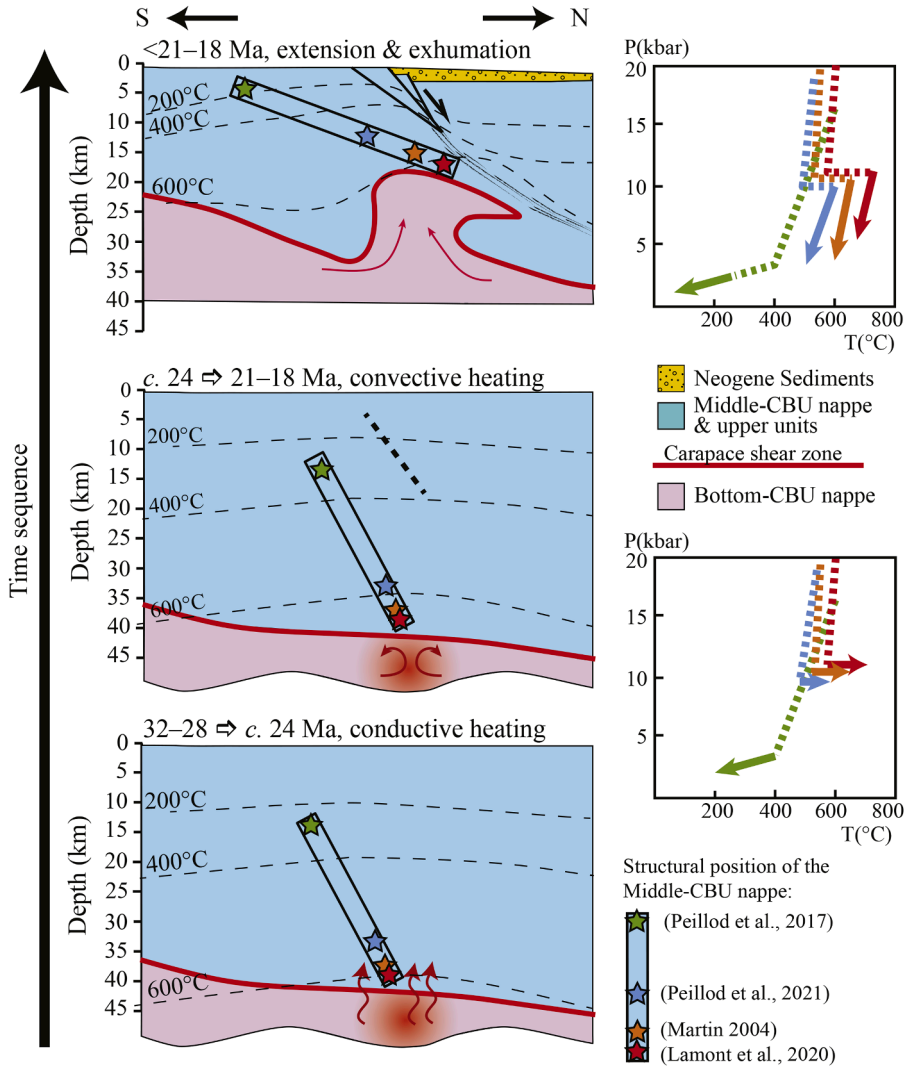

Fig. 7. Tectonic model of isobaric heating following thrusting of the Middle- onto the Bottom-CBU Nappe at 32–28 Ma, involving conductive heating and subsequent rollback-driven extension.

mylonites consistently provide early Miocene ages (e.g. Bakowsky et al., 2023; Glodny and Ring, 2022; Grasemann et al., 2018; Ring et al., 2010). Additionally, Bröcker et al. (2013) presented ages between ~34 and ~20 Ma for greenschist-facies overprints of the CBU on the islands of Syros and Sifnos. The greenschist-facies overprints strongly suggest that there were no significant vertical movements of the rocks over this relatively large period of time (i.e., near-isobaric conditions). The large age range is due to heterogeneous fluid availability for mineral equilibration in the decompressed HP rocks. Overall, there is no evidence for any large-scale extension at 32–28 Ma in the central Aegean when isobaric heating started. Therefore, we relate the duration of ~9.7 Ma for isobaric heating between 32 and 28 and 23–19 Ma to a period of modest tectonic activity during which the formerly accreted and partially exhumed rocks were transferred from the subduction-channel (or forearc) position into the backarc region where they were subsequently affected by rollback-controlled extension (Fig. 7).

All *P-T* estimates for the start of isobaric heating of the Middle-CBU nappe on Naxos are <600 °C, which is not hot enough to drive large horizontal ductile flow. Pronounced flow of mid/lower-crustal rocks is strongly aided by high temperatures (>600–700 °C) and the presence of melt (Arzi, 1978; Rosenberg and Handy, 2005). Within the Bottom-CBU nappe, convective heating and early melting may have started at <24 Ma (Vanderhaeghe et al., 2018). At this time, after ~5 Myr of heating, thermomechanical numerical models predict that convection starts when half of the crust has a viscosity lower than 10^{19} Pa/s (Louis-Napoléon et al., 2024). Peak temperatures are reached at the end of isobaric heating and thermodynamic models indicate that the Bottom-CBU nappe started to cross the solidus and produced ~7 % melt fraction (Lamont et al., 2020), which would correspond to a drastic drop of crustal strength (~90 %) associated with ductile flow (Rosenberg and Handy 2005). In the Middle-CBU nappe, peak HT metamorphism does not cross the solidus; however, ~9.7 Myr of thermal relaxation would still correspond to a ~30–40 % decrease in strength according to Glazner and Bartley (1985).

We argue that the drop in crustal strength and rock viscosity after isobaric heating controlled the style of crustal extensional deformation during rollback. Initial deposition in sedimentary basins and extensional deformation were dated at 23–19 Ma (Bakowsky et al., 2023; Grasemann et al., 2012; e.g. Kuhlemann et al., 2004) which Ring et al. (2010) interpret as the beginning of the large-scale continental extension in the Aegean due to slab rollback. Extensional exhumation was more pronounced in the central Aegean where the deepest, migmatitic parts of the Middle-CBU nappe and the Bottom-CBU nappe are exhumed.

The ~10 Myr phase of isobaric heating in the central Aegean is interpreted to reflect an interlude in the exhumation of the HP rocks when the latter were transferred from the cold subduction channel, where the early phase of exhumation during overall convergence occurred, into the hot backarc region where the late extension-

controlled exhumation stage took place. Isobaric heating caused a drop in crustal strength which guided the style of large-scale continental extension. Because rocks in slab-rollback settings must shift from the subduction zone into the backarc region, the processes discussed here might be of general importance.

Our results from a natural example of isobarically heated crust reiterates the importance of radiogenic decay of crustal material and is, thus, different to heating caused by asthenospheric upwelling as favoured by the numerical models of Sizova et al. (2019). Their numerical results well reproduce β-shaped P–T paths of ultra-HP rocks that show isobaric heating of ~>200 °C during exhumation at high/ultrahigh T (>600–900 °C), as observed, for example, in the Bohemian Massif. In contrast, the model results of Sizova et al. (2019) have difficulty to reproduce isobaric heating of 40–100 °C at 300–600 °C as observed for the Lepontine Dome in the Alps or in the Cyclades. Furthermore, we showed that isobaric heating predated slab rollback and is not a consequence of heating triggered by rollback-controlled asthenospheric upwelling. Nonetheless, our results agree with those of Sizova et al. (2019) by showing that early (preheating) segments of β-shaped *P-T* paths can be completely erased. This may lead to problems drawing tectonic conclusions as an early HP metamorphic overprint in deep parts of the crust is being overlooked and large-scale thrusts placing HP rocks onto non-HP rocks might be inferred.

CRediT authorship contribution statement

Alexandre Peillod: Writing – review & editing, Writing – original draft, Formal analysis, Data curation, Conceptualization. **Benjamin Hess:** Writing – review & editing, Writing – original draft, Formal analysis. **Evangelos Moulas:** Writing – review & editing, Formal analysis. **Simon Hector:** Writing – review & editing, Formal analysis, Data curation. **Clifford G.C. Patten:** Writing – review & editing, Formal analysis, Data curation. **Aratz Beranoaguirre:** Writing – review & editing, Formal analysis, Data curation. **Uwe Ring:** Writing – review & editing, Writing – original draft, Conceptualization.

Declaration of competing interest

The authors declare the following financial interests/personal relationships which may be considered as potential competing interests:

Alexandre Peillod reports financial support was provided by German Research Foundation. Uwe Ring reports financial support was provided by Swedish Research Council. If there are other authors, they declare that they have no known competing financial interests or personal relationships that could have appeared to influence the work reported in this paper.

Acknowledgments

We thank E. Pauthenet and the Pôle de Calcul et de Données Marines for providing DATARMOR computational resources. We acknowledge funding by the German Science Foundation (DFG projects 02020830221 and 512790090) and the Swedish Science Council (Vetenskapsrådet grant 2021–04075). We are thankful for the reviews by Dominik Sorger and an anonymous referee, which helped us to improve the manuscript as well as for the editor handling by Alex Webb. Thanks as well to Pierre Lanari and Olivier Vanderhaeghe for the useful comments.

Supplementary materials

Supplementary material associated with this article can be found, in the online version, at doi:10.1016/j.epsl.2025.119409.

Data availability

Data will be made available on request.

References

Angelier, J., Glaçon, G., Muller, C., 1978. Sur la présence et la position tectonique du miocène inférieur marin dans l'archipel de Naxos (Cyclades, Grèce). C. R. Acad. Sci 286, 21–24.

Artemieva, I.M., Thybo, H., Jakobsen, K., Sørensen, N.K., Nielsen, L.S., 2017. Heat production in granitic rocks: global analysis based on a new data compilation GRANITE2017. Sci. Rep 172, 1–26.

Arzi, A.A., 1978. Critical phenomena in the rheology of partially melted rocks. Tectonophysics 44, 173–184. https://doi.org/10.1016/0040-1951(78)90069-0.

Bakowsky, C., Schneider, D.A., Grasemann, B., Soukis, K., 2023. Miocene ductile thinning below the Folegandros Detachment System, Cyclades, Greece. Terra Nov 35, 220–229. https://doi.org/10.1111/ter.12646.

Bonneau, M., Geyssant, J., Lepvrier, C., 1978. Tectonique Alpine dans le massif d'Attique-cyclades (Gréce) plis couchés kilométriques dans l'île de Naxos. Rev. Géogr. Géol. Dyn 20, 109–122.

Borghi, A., Compagnoni, R., Sandrone, R., 1996. Composite P-T paths in the internal Penninic Massifs of the Western Alps: petrological constraints to their thermo-mechanical evolution. Eclogae Geol. Helv 89, 345–367.

Borinski, S.A., Hoppe, U., Chakraborty, S., Ganguly, J., Bhowmik, S.K., 2012. Multicomponent diffusion in garnets I: general theoretical considerations and experimental data for Fe-Mg systems. Contrib. Miner. Pet. 164, 571–586. https://doi.org/10.1007/s00410-012-0758-0.

Bovay, T., Lanari, P., Rubatto, D., Smit, M., Piccoli, F., 2022. Pressure–temperature–time evolution of subducted crust revealed by complex garnet zoning (Theodul Glacier Unit, Switzerland). J. Metamorph. Geol 40, 175–206. https://doi.org/10.1111/jmg.12623.

Brichau, S., Ring, U., Ketcham, R.A., Carter, A., Stockli, D., Brunel, M., 2006. Constraining the long-term evolution of the slip rate for a major extensional fault system in the central Aegean, Greece, using thermochronology. Earth Planet. Sci. Lett 241, 293–306. https://doi.org/10.1016/j.epsl.2005.09.065.

Bröcker, M., Baldwin, S., Arkudas, R., 2013. The geological significance of 40Ar/39Ar and Rb-Sr white mica ages from Syros and Sifnos, Greece: a record of continuous (re) crystallization during exhumation? J. Metamorph. Geol 31, 629–646. https://doi.org/10.1111/jmg.12037.

Buick, I.S., Holland, T.J.B., 1989. The P–T–t path associated with crustal extension, Naxos, Cyclades, Greece. Geol, Soc, Lond. Spec, Publ 1, 365–369. https://doi.org/10.1144/GSL.SP.1989.043.01.32.

Büttner, D., Kowalczyk, G., 1978. Late cenozoic stratigraphy and paleogeography of Greece - A review, in: Alps, Apennines, Hellenides. Geodynamic Investigations Along Geotraverses by an International Group of Geoscientists. pp. 494–501.

Caddick, M.J., Konopásek, J., Thompson, A.B., 2010. Preservation of garnet growth zoning and the duration of prograde metamorphism. J. Pet. 51, 2327–2347. https://doi.org/10.1093/petrology/egq059.

Cao, S., Neubauer, F., Bernroider, M., Genser, J., 2018. Eocene high-pressure metamorphism and oligocene retrogression on Naxos, Cyclades, Greece: significance for aegean tectonics and 40Ar/39Ar dating in polyphase metamorphic rocks. Tectonophysics 745, 66–94. https://doi.org/10.1016/j.tecto.2018.08.009.

Duchêne, S., Aïssa, R., Vanderhaeghe, O., 2006. Pressure-temperature-time evolution of metamorphic rocks from Naxos (Cyclades, Greece): constraints from thermobarometry and Rb/Sr dating. Geodin. Acta 19, 299–319.

England, P.C., Thompson, A.B., 1984. Pressure-temperature-time paths of regional metamorphism II: their inference and interpretation using mineral assemblages in metamorphis rocks. J. Pet. 25, 929–955. https://doi.org/10.1093/petrology/25.4.929.

Faryad, S.W., Baldwin, S.L., Jedlicka, R., Ježek, J., 2019. Two-stage garnet growth in coesite eclogite from the southeastern Papua New Guinea (U)HP terrane and its geodynamic significance. Contrib, Miner., Pet. 174. https://doi.org/10.1007/s00410-019-1612-4.

Feenstra, A., 1985. Metamorphism of bauxites on Naxos, Greece. Dr. Diss. Inst. Voor aardwetenschappen RUU.

Flansburg, M.E., Stockli, D.F., Poulaki, E.M., Soukis, K., 2019. Tectono-magmatic and stratigraphic evolution of the Cycladic Basement, Ios Island, Greece. Tectonics 38, 2291–2316. https://doi.org/10.1029/2018TC005436.

Forster, M., Koudashev, O., Nie, R., Yeung, S., Lister, G., 2020. 40Ar/39Ar thermochronology in the Ios basement terrane resolves the tectonic significance of the south Cyclades Shear Zone. Geol, Soc, Spec, Publ 487, 291–313. https://doi.org/10.1144/SP487-2018-169.

Glazner, A.F., Bartley, J.M., 1985. Evolution of lithospheric strength after thrusting. Geology 13, 42–45. https://doi.org/10.1130/0091-7613(1985)13<42:EOLSAT>2.0.CO;2.

Glodny, J., Ring, U., 2022. The Cycladic Blueschist Unit of the Hellenic subduction orogen: protracted high-pressure metamorphism, decompression and reimbrication of a diachronous nappe stack. Earth-Sci. Rev 224. https://doi.org/10.1016/j.earscirev.2021.103883.

Grasemann, B., Huet, B., Schneider, D.A., Rice, A.H.N., Lemonnier, N., Tschegg, C., 2018. Miocene postorogenic extension of the Eocene synorogenic imbricated Hellenic subduction channel: new constraints from Milos (Cyclades, Greece). Bull, Geol, Soc, Am 130, 238–262. https://doi.org/10.1130/B31731.1.

Grasemann, B., Schneider, D.A., Stöckli, D.F., Iglseder, C., 2012. Miocene bivergent crustal extension in the Aegean: evidence from the western Cyclades (Greece). Lithosphere 4, 23–39. https://doi.org/10.1130/L164.1.

Hecht, J., 1979. Geologische Karte des Schmirgel-fuËhrenden Gebietes zwischen Apiranthos und Koronos, Naxos, Griechenland; 1:10000. Institute for Geology and Mineral Resources, Athens.

Henjes-Kunst, F., Altherr, R., Kreuzer, H., Hansen, B.T., 1988. Disturbed UThPb systematics of young zircons and uranothorites: the case of the Miocene Aegean granitoids (Greece). Chem, Geol, Isot, Geosci, Sect 73, 125–145. https://doi.org/10.1016/0168-9622(88)90011-5.

Henk, A., von Blanckenburg, F., Finger, F., Schaltegger, U., Zulauf, G., 2000. Syn-convergent high-temperature metamorphism and magmatism in the Variscides: a discussion of potential heat sources. Geol, Soc, Spec, Publ 179, 387–399. https://doi.org/10.1144/GSL.SP.2000.179.01.23.

Huet, B., Labrousse, L., Monié, P., Malvoisin, B., Jolivet, L., 2015. Coupled phengite 40Ar-39Ar geochronology and thermobarometry: p-T-t evolution of Andros Island (Cyclades, Greece). Geol, Mag 152, 711–727. https://doi.org/10.1017/S0016756814000661.

Huet, B., Le Pourhiet, L., Labrousse, L., Burov, E.B., Jolivet, L., 2011. Formation of metamorphic core complex in inherited wedges: a thermomechanical modelling study. Earth Planet, Sci, Lett 309, 249–257. https://doi.org/10.1016/j.epsl.2011.07.004.

Jansen, J.B.H., Schuiling, R.D., 1976. Metamorphism on Naxos petrology and geothermal gradient. Am, J. Sci 276, 1225–1253. https://doi.org/10.2475/ajs.276.10.1225.

Jolivet, L., Brun, J.P., 2010. Cenozoic geodynamic evolution of the Aegean. Int, J. Earth Sci 99, 109–138. https://doi.org/10.1007/s00531-008-0366-4.

Jolivet, L., Lecomte, E., Huet, B., Denèle, Y., Lacombe, O., Labrousse, L., Le Pourhiet, L., Mehl, C., 2010. The North cycladic Detachment System. Earth Planet, Sci, Lett 289, 87–104. https://doi.org/10.1016/j.epsl.2009.10.032.

Keay, S., Lister, G., Buick, I., 2001. The timing of partial melting, Barrovian metamorphism and granite intrusion in the Naxos metamorphic core complex, Cyclades, Aegean Sea, Greece. Tectonophysics 342, 275–312. https://doi.org/10.1016/S0040-1951(01)00168-8.

Kuhlemann, J., Frisch, W., Dunkl, I., Kázmér, M., Schmiedl, G., 2004. Miocene siliciclastic deposits of Naxos Island: geodynamic and environmental implications for the evolution of the southern Aegean Sea (Greece). Spec, Pap, Geol, Soc, Am 378, 51–65. https://doi.org/10.1130/0-8137-2378-7.51.

Lamont, T.N., Searle, M.P., Waters, D.J., Roberts, N.M.W., Palin, R.M., Smye, A., Dyck, B., Gopon, P., Weller, O.M., St-Onge, M.R., 2020. Compressional origin of the Naxos metamorphic core complex, greece: structure, petrography, and thermobarometry. Bull, Geol, Soc, Am 132, 149–197. https://doi.org/10.1130/B31978.1.

Laurent, V., Lanari, P., Naïr, I., Augier, R., Lahfid, A., Jolivet, L., 2018. Exhumation of eclogite and blueschist (Cyclades, Greece): pressure–temperature evolution determined by thermobarometry and garnet equilibrium modelling. J. Metamorph, Geol 36, 769–798. https://doi.org/10.1111/jmg.12309.

Lister, G.S., Forster, M.A., 1996. Inside the aegean metamorphic core complexes : a field trip guide illustrating the geology of 27, 41–46. https://doi.org/10.3809/doi.

Liu, Q., Hermann, J., Zhang, J., 2013. Polyphase inclusions in the Shuanghe UHP eclogites formed by subsolidus transformation and incipient melting during exhumation of deeply subducted crust. Lithos 177, 91–109. https://doi.org/10.1016/j.lithos.2013.06.010.

Louis-Napoléon, A., Vanderhaeghe, O., Gerbault, M., Martin, R., Bonometti, T., 2024. Formation of the Naxos nested domes by convection and diapirism. BSGF - Earth Sci, Bull 1–15. https://doi.org/10.1051/bsgf/2024017.

Martin, L., 2004. Martin, L. (2004). Signification des âges U-Pb sur zircon dans l'histoire métamorphique de Naxos et Ikaria (Cyclades, Grèce). Université Henri Poincaré, Nancy 1.

Martin, L., Duchêne, S., Deloule, E., Vanderhaeghe, O., 2006. The isotopic composition of zircon and garnet: a record of the metamorphic history of Naxos, Greece. Lithos 87, 174–192. https://doi.org/10.1016/j.lithos.2005.06.016.

Moulas, E., Schorn, S., 2024. T1dH : a 1-d code for the calculation of heat conduction with Earth Science Applications (1.0). Zenodo. https://doi.org/10.5281/zenodo.11046566.

Parra, T., Vidal, O., Jolivet, L., 2002. Relation between the intensity of deformation and retrogression in blueschist metapelites of Tinos Island (Greece) evidenced by chlorite-mica local equilibria. Lithos 63, 41–66. https://doi.org/10.1016/S0024-4937(02)00115-9.

Patten, C.G.C., Beranoaguirre, A., Hector, S., Gudelius, D., Kolb, J., Eiche, E., 2023. Improved whole rock low detection limit gold analysis by LA-ICP-MS utilizing pressed-powder-pellets. Int, J. Mass Spectrom 488, 117039.

Peillod, A., 2018. The metamorphic history of Naxos (central Cyclades, Greece): Deciphering the Oligocene and Miocene exhumation events. Stockholm University.

Peillod, A., Majka, J., Ring, U., Drüppel, K., Patten, C., Karlsson, A., Włodek, A., Tehler, E., 2021a. Differences in decompression of a high-pressure unit: a case study from the Cycladic Blueschist Unit on Naxos Island, Greece. Lithos 386–387. https://doi.org/10.1016/j.lithos.2021.106043.

Peillod, A., Patten, C.G.C., Drüppel, K., Beranoaguirre, A., Zeh, A., Gudelius, D., Hector, S., Majka, J., Kleine-Marshall, B.I., Karlson, A., Gerdes, A., Kolb, J., 2024. Disruption of a high-pressure unit during exhumation: example of the Cycladic Blueschist unit (Thera, Ios and Naxos islands, Greece). J. Metamorph, Geol 42, 225–255. https://doi.org/10.1111/jmg.12753.

Peillod, A., Ring, U., Glodny, J., Skelton, A., 2017. An eocene/oligocene blueschist-/greenschist facies P–T loop from the Cycladic Blueschist Unit on Naxos Island, Greece: deformation-related re-equilibration vs. thermal relaxation. J. Metamorph, Geol 35, 805–830. https://doi.org/10.1111/jmg.12256.

Peillod, A., Tehler, E., Ring, U., 2021b. Quo vadis Zeus : is there a Zas shear zone on Naxos Island, Aegean Sea, Greece? A review of metamorphic history and new kinematic data. J. Geol, Soc, Lond. 178, jgs2020–jgs2217. https://doi.org/10.1144/jgs2020-217.

Perraki, M., Faryad, S.W., 2014. First finding of microdiamond, coesite and other UHP phases in felsic granulites in the Moldanubian Zone: implications for deep subduction and a revised geodynamic model for Variscan Orogeny in the Bohemian Massif. Lithos 202–203, 157–166. https://doi.org/10.1016/j.lithos.2014.05.025.

Reischmann, T., 1998. Pre-Alpine origine of tectonic units from the metamorphic complex of Naxos, Greece, identified by single zircon Pb/Pb dating. Bull. Geol. Soc. Greece XXXII/3, 101–111.

Ring, U., Glodny, J., Peillod, A., Skelton, A., 2018. The timing of high-temperature conditions and ductile shearing in the footwall of the Naxos extensional fault system, Aegean Sea, Greece. Tectonophysics 745, 366–381. https://doi.org/10.1016/j.tecto.2018.09.001.

Ring, U., Glodny, J., Will, T., Thomson, S., 2010. The hellenic subduction system: high-pressure metamorphism, exhumation, normal faulting, and large-scale extension. Annu, Rev, Earth Planet, Sci 38, 45–76. https://doi.org/10.1146/annurev.earth.050708.170910.

Ring, U., Laws, S., Bernet, M., 1999. Structural analysis of a complex nappe sequence and late-orogenic basins from the Aegean Island of Samos, Greece. J. Struct, Geol 21, 1575–1601. https://doi.org/10.1016/S0191-8141(99)00108-X.

Roesler, G., 1978. Relics of non-metamorphic sediments on central Aegean islands, in: Alps, Apennines, Hellenides. Geodynamic Investigations Along Geotraverses by an International Group of Geoscientists. pp. 480–481.

Rosenberg, C.L., Handy, M.R., 2005. Experimental deformation of partially melted granite revisited: implications for the continental crust. J. Metamorph, Geol 23, 19–28. https://doi.org/10.1111/j.1525-1314.2005.00555.x.

Rybach, L., 1988. Determination of heat production rate. Handbook of terrestrial heat-flow density determination.

Ryan, P.D., Dewey, J.F., 2019. The sources of metamorphic heat during collisional orogeny: The barrovian enigma. Can. J. Earth Sci. 56, 1309–1317. https://doi.org/10.1139/cjes-2018-0182.

Scheffer, C., Vanderhaeghe, O., Lanari, P., Tarantola, A., Ponthus, L., Photiades, A., France, L., 2016. Syn- to post-orogenic exhumation of metamorphic nappes: structure and thermobarometry of the western Attic-Cycladic metamorphic complex (Lavrion, Greece). J. Geodyn 96, 174–193. https://doi.org/10.1016/j.jog.2015.08.005.

Schenker, F.L., Gerya, T., Burg, J.P., 2012. Bimodal behavior of extended continental lithosphere: modeling insight and application to thermal history of migmatitic core complexes. Tectonophysics 579, 88–103. https://doi.org/10.1016/j.tecto.2012.07.002.

Sizova, E., Hauzenberger, C., Fritz, H., Faryad, S.W., Gerya, T., 2019. Late orogenic heating of (Ultra)high pressure rocks: slab Rollback vs. Slab break., Geosci 9, 1–26. https://doi.org/10.3390/geosciences9120499.

van der Maar, P.A., Jansen, J.B.H., 1983. The geology of the polymetamorphic complex of Ios, Cyclades, Greece and its significance for the Cycladic Massif. Geol, Rundsch. 72, 283–299. https://doi.org/10.1007/BF01765910.

Vanderhaeghe, O., 2012. The thermal-mechanical evolution of crustal orogenic belts at convergent plate boundaries: a reappraisal of the orogenic cycle. J. Geodyn 56–57, 124–145. https://doi.org/10.1016/j.jog.2011.10.004.

Vanderhaeghe, O., Hibsch, C., Siebenaller, L., Martin, L., Duchêne, S., Blanquat, deS.M., Kruckenberg, S., Fotiadis, A., 2007. GUIDE, Naxos Field, PENROSE CONFERENCE EXTENDING A CONTINENT.

Vanderhaeghe, O., Kruckenberg, S.C., Gerbault, M., Martin, L., Duchêne, S., Deloule, E., 2018. Crustal-scale convection and diapiric upwelling of a partially molten orogenic root (Naxos dome, Greece). Tectonophysics 746, 459–469. https://doi.org/10.1016/j.tecto.2018.03.007.

Villa, I.M., Glodny, J., Peillod, A., Skelton, A., Ring, U., 2023. Petrochronology of polygenetic white micas (Naxos, Greece). J. Metamorph, Geol 41, 401–423. https://doi.org/10.1111/jmg.12700.

Wiederkehr, M., Bousquet, R., Schmid, S.M., Berger, A., 2008. From subduction to collision: thermal overprint of HP/LT meta-sediments in the north-eastern Lepontine Dome (Swiss Alps) and consequences regarding the tectono-metamorphic evolution of the Alpine orogenic wedge. Swiss J. Geosci 101. https://doi.org/10.1007/s00015-008-1289-6.

Wijbrans, J.R., McDougall, I., 1988. Metamorphic evolution of the Attic Cycladic Metamorphic Belt. J. Metamorph, Geol 6, 571–594.

Wilke, F.D.H., O'Brien, P.J., Gerdes, A., Timmerman, M.J., Sudo, M., Khan, M.A., 2010. The multistage exhumation history of the Kaghan Valley UHP series, NW Himalaya, Pakistan from U-Pb and 40Ar/39Ar ages. Eur, J. Miner. 22, 703–719. https://doi.org/10.1127/0935-1221/2010/0022-2051.

Zlatkin, O., Avigad, D., Gerdes, A., 2018. New detrital Zircon geochronology from the cycladic basement (Greece): implications for the paleozoic accretion of Peri-Gondwanan terranes to Laurussia. Tectonics 37, 4679–4699. https://doi.org/10.1029/2018TC005046.